Accepted Manuscript

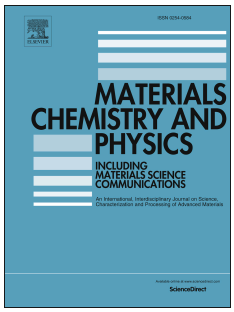

Molecular dynamics simulations on heterogeneity and percolation of epoxy nanofilm during glass transition process

Zhikun Wang, Qiang Lv, Shenghui Chen, Roland Faller, Chunling Li, Shuangqing Sun, Songqing Hu

PII: S0254-0584(18)30302-X

DOI: 10.1016/j.matchemphys.2018.04.040

Reference: MAC 20535

To appear in: *Materials Chemistry and Physics*

Received Date: 20 August 2017

Revised Date: 31 January 2018

Accepted Date: 7 April 2018

Please cite this article as: Z. Wang, Q. Lv, S. Chen, R. Faller, C. Li, S. Sun, S. Hu, Molecular dynamics simulations on heterogeneity and percolation of epoxy nanofilm during glass transition process, *Materials Chemistry and Physics* (2018), doi: 10.1016/j.matchemphys.2018.04.040.

GRAPHIC ABSTRACT

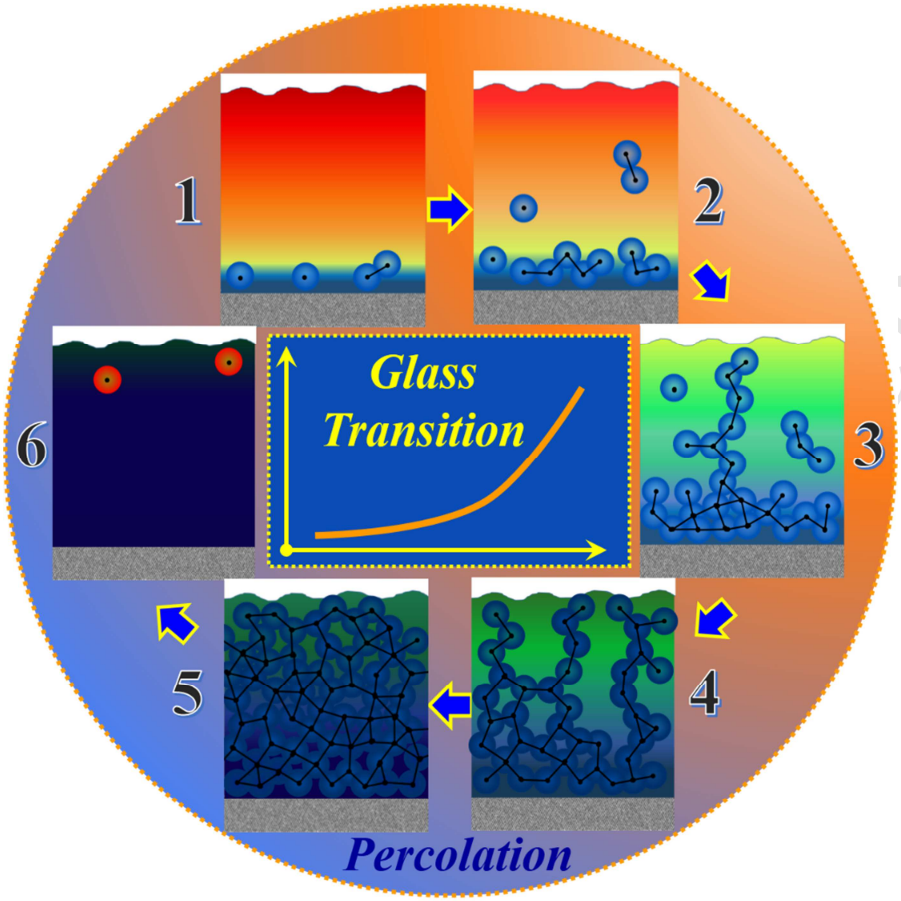

Molecular Dynamics Simulations on Heterogeneity and Percolation of Epoxy Nanofilm during Glass Transition Process

Zhikun Wang,[1,2] Qiang Lv,[1] Shenghui Chen,[1] Roland Faller,[2] Chunling Li,[1,3] Shuangqing Sun,[1,3,*] Songqing Hu[1,3,*]

[1]College of Science, China University of Petroleum (East China), Qingdao, Shandong, 266580, China

[2]Department of Chemical Engineering, UC Davis, Davis, California, 95616, USA

[3]Key Laboratory of New Energy Physics & Materials Science in Universities of Shandong, China University of Petroleum (East China), Qingdao, Shandong, 266580, China

ABSTRACT

This study uses an all-atom computational model to investigate the temperature dependent heterogeneity and percolation in a nanofilm system of short linear epoxy chains on a solid graphene surface. The heterogeneity, which indicates having physical characters that vary within the nanofilm, is mainly manifested in distributions of volume, energy and the dynamic properties. Local glass transition temperatures, T_gs, from above properties depend largely on the separation to the graphene surface, and the glass transition of the nanofilm is asynchronous along the film normal. Distinct T_g increases and decreases are particularly observed in the solid and free interfaces, respectively, compared with the bulk. From the dynamic heterogeneity, percolation effect, which indicates the connectivity of mobile and immobile domains, of the nanofilm is also observed during glass transition by plotting internal atomic mobility distribution diagrams. A multi-stage percolation mechanism based on the glass transition state and the connection state of immobile and mobile domains of the nanofilm is developed. A relatively immobile domain near the graphene surface is observed, even at temperatures much higher than T_g, and it initiates the dynamic percolation. The interconnection of immobile domains after percolation accelerate the transition from the rubbery to the glassy state.

KEYWORDS: glass transition; dynamic percolation; polymer nanofilm

* Corresponding author. College of Science, China University of Petroleum (East China), Qingdao, Shandong, 266580, China
E-mail address: sunshuangqing@upc.edu.cn (S.Q. Sun); songqinghu@upc.edu.cn (S.Q. Hu).

1. Introduction

The glass transition temperature, T_g, is a significant technological parameter since it is the temperature at which most polymers freeze into a glassy state. Over the past decade there has been considerable interest in the effect of chemical structure or environment on the glass transition behavior in thin polymeric films[1-7]. This has important implications for friction, lubrication, adhesion and other applications involving polymer surfaces as the glass transition in thin films is highly relevant for many processes such as coating and printing[8-11]. The overall T_g in polymer nanofilms has been reported to be dependent on the interplay of the bulk, the solid interface and the free interface. Most recent reports are consistent with a region with reduced mobility at the solid interface due to the steric hindrance of the substrate surface and the decreased configurational space for molecular motions, as well as a region with enhanced mobility at the free interface due to the relaxation of the constraints to molecular motions. Interfaces can induce strong dynamical heterogeneity in nanofilms[12-15].

The heterogeneity of the nanofilm depends largely on the interfacial regions in the nanofilm, especially for systems confined by solid surfaces or nanoparticles. The performance inconsistency between interfacial regions (i.e., solid or free interfaces) and bulk leads to difficulties in predicting overall properties[16,17]. Many current research efforts focus on quantitatively understanding the effect of interfacial areas on the overall thermodynamic properties of the nanofilms during the glass transition. Forrest et al.[18-20] provide strong direct evidence for the existence of a relaxed free interface region in a polymer nanofilm supported by a solid surface on one side and air on the other. They point out that during cooling, the polymer nanofilm transits from whole-film flow to surface localized flow over a narrow

temperature region near the bulk T_g. By studying the localized dynamics in a nanocomposite system, Khare et al[21-23] reported that solid interfaces with more immobile atoms than the bulk will restrain the whole-flow of the polymer bulk and increase the overall T_g. Therefore, the solid and free interfaces in confined polymer nanofilms, which significantly lead to the dynamic heterogeneity of a system, have opposite effects on the glass transition.

Molecular dynamics (MD) has been used to study the internal microscopic mechanisms of nanofilms since it can reveal detailed structural or dynamical properties of the interfaces[24-27]. Morita et al.[8] performed coarse-grained MD to illustrate the thermodynamic and dynamic relations between free interface and bulk regions in a polymer film. Their results show that polymers in the free interface region move faster than in the bulk decreasing the T_g of the free interface. Ndoro et al.[28] adopted all-atom MD to study the effect of a solid surface on the dynamic properties of atoms in the solid interface region. They observed a gradual increase in the mobility of atoms from the solid surface to the bulk by computing the mean square displacements (MSDs), indicating a large dynamic heterogeneity in the solid interface regions. Eslami et al.[23] studied the internal structure and dynamic heterogeneous properties of polymers in both solid and free interface regions by coarse grained MD. They proposed that different structure or dynamic parameters of the interface, e.g., chain conformation, mass distribution, hydrogen dynamic, chain translation etc. yield different interface thicknesses, which reveals the complexity of glass transition properties in nanoscale interfaces. All MD simulation studies on interfacial properties of confined polymer systems provide good explanations to the heterogeneous property of the overall polymer nanofilm.

To further develop theories on the heterogeneity of the polymer system, Long et al.[29-31]

hypothesized that the polymer system is composed of mobile and immobile domains. Upon cooling, the immobile domains grow at the expense of the mobile ones and the glass transition occurs when the immobile domains percolate through the polymer matrix. Then, the percolated domains substantially reduce the atomic mobility in the whole system and the polymer matrix freezes into glassy state. This percolation mechanism correlates the glass transition to the internal dynamics of the overall system[29,32]. For polymer nanofilms, the dynamic heterogeneity of the overall system largely depends on the location and extent of solid and free interface regions. The interfacial regions in nanofilm systems play a significant role in initiating the percolation of the system during the glass transition[33,34].

Although the existing mechanisms based on the heterogeneity or percolation properties can provide important insight for understanding the localized glass transition behavior of polymer nanofilms, there is still much to be learned due to the complexity of physical or chemical properties of polymer materials[29]. In particular, we need more accurate observations on the molecular or atomic level to support or develop mechanisms. It is the purpose of this study to provide further insights into the heterogeneity and percolation of a nanofilm composed of epoxy resins during the glass transition. All-atom MD is used to capture the molecular-level properties of the epoxy resin nanofilm. This work aims to answer two questions: (1) what effects do the internal volume, energy and dynamic heterogeneities have on the overall glass transition of the epoxy nanofilm; (2) how does the glass transition of the epoxy resin nanofilm depend on the percolation in the nanofilm.

2. Model and Simulation Details

MD is a computer simulation method for qualitative and quantitative description of the physical movements of atoms and molecules, giving the dynamic evolution of a model during a fixed period of time. All modeling and simulations in this work were performed using a commercial software package called Materials Studio (Accelrys Inc). We constructed an epoxy resin nanofilm in contact with a 4-layer graphene surface on one side and vacuum on the other. The epoxy resin nanofilm consists of diglycidyl ether bisphenol A (DGEBA) as the epoxy monomer and cyclohexylamine (CHA) as the cross-linker. 4 DGEBA and 4 CHA monomers were used to construct a short epoxy chain through the ring-opening reaction between the epoxy group on DGEBA and the amino group on CHA[21]. 30 epoxy chains were used to form the overall nanofilm. Periodic boundary conditions were applied to the *x* and *y* (in plane) directions of the simulation box. Along the *z* axis, a 60 Å thick vacuum layer was added which allows thermal expansion of the nanofilm in this direction, but avoids migration of epoxy chains out of the film. A 10000 iteration step geometry minimization was first performed on the model until energies and forces converged below a tolerance of E = 0.001 kcal/mol and f = 0.5 kcal/mol/Å. Then, a 3 ns NVT (constant atom number, system volume and temperature) simulation was conducted at 640 K, to remove residual stresses and obtain an energy stabilized state. The graphene surface was constrained during all minimizations and NVT simulations. The chemical structures of the model components and the final equilibrium model are shown in Fig. 1.

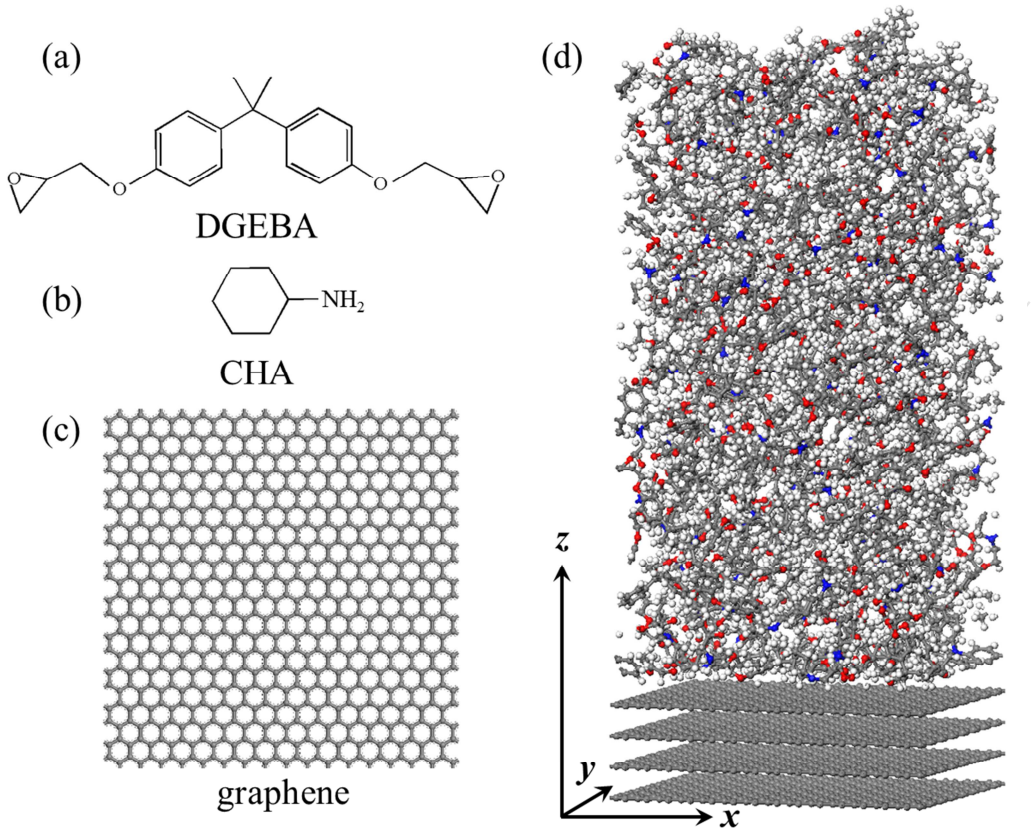

Fig. 1. Schematic illustration of the model components and the equilibrium model. (a) diglycidyl ether bisphenol A (DGEBA); (b) cyclohexylamine (CHA); (c) graphere; (d) model of epoxy resin nanofilm on the 4-layer graphere surface. The gray, white, red and blue beads in the equilibrium model indicates the carbon, hydrogen, oxygen and nitrogen atoms, respectively. The box border and the vacuum layer are hidden for clarity.

In order to study the glass transition behavior of the epoxy nanofilm, a stepwise cooling was performed. In previous studies[21,35], we have performed similar simulations on pure epoxy and epoxy/SiO_2 nanocomposite models and validated them against experiments and other simulations. Here, we cooled down the system from 640 K to 300 K at a rate of 20 K/ns. This means that constant NVT MD was performed every 20 K for 1 ns and 1000 snapshots were stored for later data processing. During data collection, the last 500 ps at each temperature

was used to compute the equilibrium volume, energy or dynamic properties (except for the *MSD* which was calculated over the full 1 ns). It should be noted that the epoxy nanofilm was allowed to shrink or expand along the film normal during cooling, leading to variations in the density distribution. The Nosé-Hoover thermostat[36] (*Q* ratio = 0.01) was used to control the temperature. The graphene surface was constrained during cooling. For improved sampling, the entire process including model construction, stabilization and cooling was repeated three times, and the obtained calculation results are averaged.

Table 1

Input and control parameters for all modeling and simulations

Initial equilibrium	**Glass transition**
Geometry: energy tolerance *E* = 0.001 kcal/mol	Start temperature = 640 K
force tolerance *f* = 0.5 kcal/mol/Å	End temperature = 300 K
max iteration = 10000	Cooling rate = 20 K/ns
Dynamic: time = 3 ns	time step = 1 fs
time step = 1 fs	ensemble = NVT
temperature = 640 K	thermostat = Nosé-Hoover (*Q* ratio 0.01)
ensemble = NVT	
thermostat = Nosé-Hoover (*Q* ratio 0.01)	
Force field: COMPASS	
Ewald summation for electrostatic: accuracy = 0.001 kcal mol^{-1}	
Atom based summation for van der Waals: cutoff distance = 12.5 Å	

To verify that the box size we use does not create problems, a relative larger model than the one here was considered and the structural and dynamical properties of them are compared (Figure S1 in Supporting Information), and the results indicates that the box size we use are large enough for our simulations. A velocity Verlet algorithm[37] with a time step of 1 fs was with the COMPASS[38] force field to describe the inter- and intramolecular forces. The atom-based method with a cutoff distance of 12.5 Å was used to calculate the van der Waals energy, while the Ewald[39] method with an accuracy of 0.001 kcal mol^{-1} was used to calculate the Coulomb energy. All input and control parameters for all modeling and simulations are listed in Table 1.

3. Results and Discussion

3.1. Mass Density Profiles

Mass density profiles were measured to illustrate the overall mass distributions of epoxy resin atoms on the graphene surface (Fig. 2a). The density profiles were evaluated in approximately 0.05 nm thick slabs along the film normal, and the data was averaged over the last 500 ps of the trajectory at each simulated temperature. The nanofilm can be divided into three distinct regions throughout cooling: solid interface region, bulk region and free interface region. Specifically, the mass density between d_z = 15 Å to d_z = 30 Å has two distinct peaks, showing a layered solid interface feature. The mass density arrives at a constant value at d_z = 30 Å from the graphene surface and remains unchanged with increasing distance, corresponding to bulk behavior. Approaching vacuum, the mass density starts to drop and finally reaches zero, this drop represents the free surface. Such a regional division is

consistent with previous reports[23,40] of similar models. Note that the density profile was normalized by the averaged bulk density at each temperature.

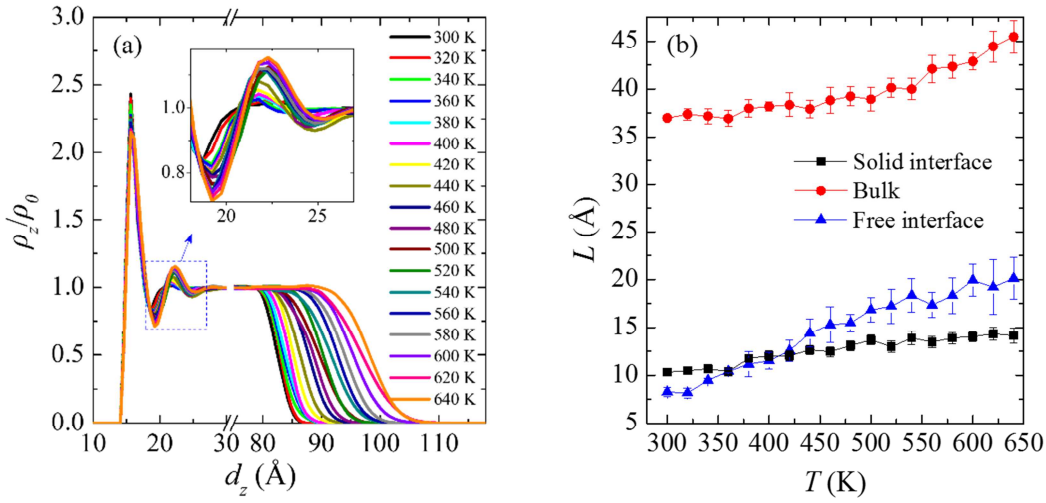

Fig. 2. Temperature dependent (a) normalized mass density distributions of the epoxy nanofilm in the *z* direction of the box, and (b) thicknesses of the solid interface, bulk and free interface. Inset in (a): enlarged profiles from 18 Å to 27 Å.

The two peaks in the layered solid interface are temperature dependent. The first peak at d_z = 15 Å slightly increases during cooling as with lower thermal mobility atoms tend to aggregate more closely at the solid surface[40]. However, the second peak at d_z = 22 Å stays constant from 640 K to 440 K but is reduced to almost bulk value from 440 K to 300 K. The two peaks appear to have opposite temperature dependence. In the low temperature range, the bulk density fluctuates heavily and it becomes harder to distinguish the second peak from the bulk, which resulted from not having enough relaxation time at each simulated temperature.

In addition, the thicknesses of the solid interface (L_{solid}), bulk (L_{bulk}) and free interface (L_{free}) regions are also temperature dependent (Fig. 2b). L_{solid} is calculated from the graphene

surface (at d_z = 15 Å) to where the density reaches the bulk value after the second peak. L_{bulk} is calculated from the edge of the solid interface to where it starts to drop, i.e., $\rho_z/\rho_0 < 1.0$, near the free interface. L_{free} is calculated from where the bulk density starts to drop to where it reaches zero. The thicknesses of the three regions are all reduced by decreasing temperature. Particularly, L_{solid} drops from 14 Å to 10 Å over our temperature range, consistent with our earlier work[21]. L_{bulk} decreases from 46 Å to 37 Å, indicating shrinkage of the film during cooling. L_{free} is reduced from 20 Å to 8 Å, reflecting the weak restriction effect of the vacuum on the epoxy nanofilm. Previous atomistic and coarse-grained simulations[22,31,41,42] reported similar temperature dependent behaviors of the bulk or interface thicknesses defined by either structural or dynamical properties of polymeric materials.

3.2. Heterogeneity of the Nanofilm during Glass Transition

3.2.1. Volume Properties

The glass transition behavior of the nanofilm was first studied by analyzing the temperature dependence of the total volume (*V*) and the fractional free volume (*FFV*) of the model (Fig. 3). *V* is defined as the volume from the graphene surface to where the density drops to half of the bulk value in the free interface region. *FFV* is obtained by calculating the free volume as a percentage of *V*, using the "Atom Volume & Surfaces" tool (Connolly radius equals 1.0 Å) in the Material Studio software. A larger *FFV* indicates that the model provides more space for atomic motion.

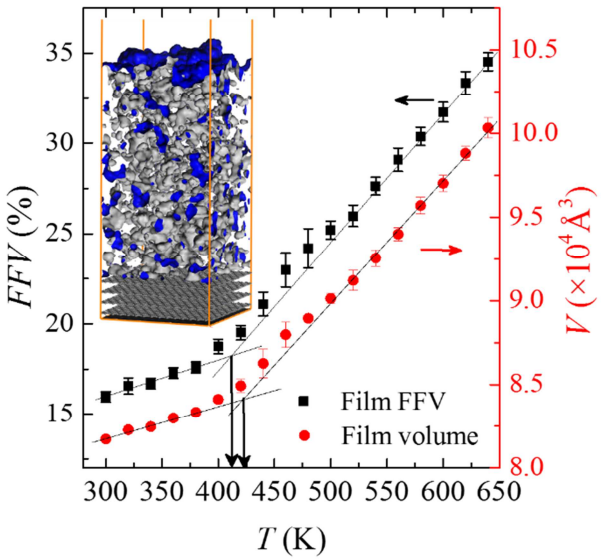

Fig. 3. Fractional free volume and total volume of the nanofilm as a function of temperature. Inset: an example of the internal free volume distribution, in which gray and blue regions indicate the free volume and the border of the free volume, respectively.

It is observed that during cooling, V is reduced from 10.03×10^4 Å^3 to 8.17×10^4 Å^3, meanwhile *FFV* is reduced from 34.53% to 15.96%. Both values drop in two stages, with larger and smaller slopes in higher and lower temperature ranges, respectively. This behavior is commonly considered a hallmark of the glass transition of polymeric systems, or the transition from rubbery state to glassy state[43]. A temperature interval of 80 K is used to linearly fit in these two regions (i.e., 640 K ~ 560 K and 380 K ~ 300 K), and the temperature at the intersection of these two fits is taken as the glass transition temperature (T_g). The obtained T_g values from V and *FFV* are $T_{g,\,V}$ = 422 ± 11 K and $T_{g,\,FFV}$ = 412 ± 7 K, respectively (Table 2). The close T_gs and similar transition trends of V - T and *FFV* - T relations indicate that free volume plays an essential role in the volumetric glass transition. Fox and Flory[44] have reported that a relatively larger *FFV* in a rubbery polymer increases the

probability for atomic motion and chain configuration changes. The smaller *FFV* in glassy polymers slows down the atomic and chain motions since the free volume in glassy polymer will be "frozen", and local polymer segments can only fluctuate around their equilibrium position[45]. Such transition behaviors of the free volume near T_g has been reported earlier for both linear[46] and cross-linked[35] polymeric systems.

Table 2

Glass transition temperatures (T_g) obtained from volume, energy and dynamic properties. (K)

Volume		Energy		Dynamic			
$T_{g,\,FFV}$	412 ± 7	$T_{g,\,nonbond}$	416 ± 9	$T_{g,\,D}$	467 ± 13	T_g [b]	345
$T_{g,\,V}$	422 ± 11	$T_{g,\,vdW}$	408 ± 7	$T_{g,\,P}$	460 ± 20		
$T_{g,SV,solid}$	485 ± 13	$T_{g,HB,solid}$	457 ± 11	$T_{g,\,Rg}$	488 ± 13, 469 ± 18,		
$T_{g,SV,bulk}$	440 ± 17	$T_{g,HB,bulk}$	425 ± 13		454 ± 16, 443 ± 13,		
$T_{g,SV,free}$	392 ± 15	$T_{g,HB,free}$	405 ± 19		440 ± 11, 437 ± 11, 423 ± 23 [a]		

[a] The $T_{g,\,Rg}$ values of the 7 slabs from graphene to vacuum.

[b] The T_g of the crosslinked DGEBA/CHA bulk system tested by dynamic scanning calorimetry[47].

The local free volume distribution is greatly dependent on the extent of the dense solid interface and the free interface along *z* axis of the model. This will inevitably lead to heterogeneous glass transition behaviors of different local regions in the nanofilm. A recent

study[21] in our group has pointed out that the reduced mobility of epoxy atoms in a denser interface will trigger the glass transition (i.e., increase T_g) of the bulk, while the increased mobility of epoxy atoms in a looser interface will restrain the glass transition (i.e., decrease T_g) of the bulk. Specific volume heterogeneity is expected to play an important role in driving the glass transition of the total film. To verify this, the nanofilm is divided into 10 Å thick slabs along the *z* axis and the specific volumes (*SV*s, inverse of density) of 7 representative slabs are monitored as a function of temperature (Fig. 4). Based on the mass density profiles (Fig. 2a), the 15 Å ~ 25 Å slab corresponds to the solid interface, the 5 slabs from 25 Å to 75 Å are in the bulk, and the slab of the "last 10 Å" corresponds to the free interface. The "last 10 Å" represents the 10 Å slab whose outer side locates to the position where the density drops to half of the bulk value in the free interface region at each simulated temperature.

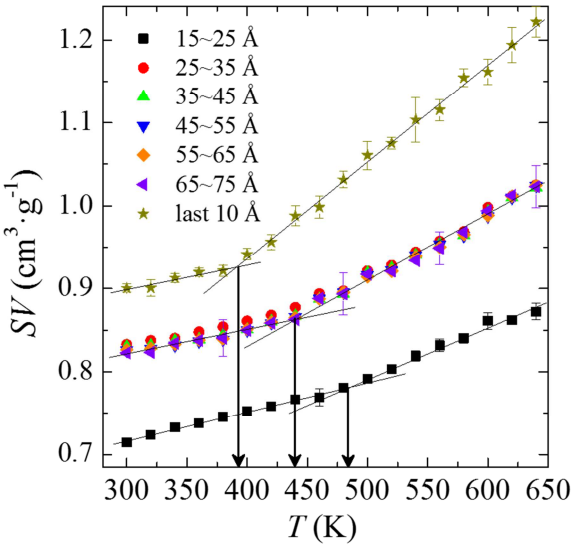

Fig. 4. Local specific volume of the nanofilm as a function of *z*. For clarity of details, not all error bars are shown.

The bulk region (i.e., 25 ~ 75 Å) has a significantly higher *SV* (lower density) than the solid interface (15 ~ 25 Å) but a significantly lower *SV* (higher density) than the free interface (i.e., last 10 Å). This is due to the effect that the solid interface can restrain atomic motion and conformational transition and aggregate atoms nearby, while the vacuum frees these motions and decreases the aggregation of chains in the free interface. The *SV* - *T* relation of the bulk appears to be more gradual than in the free interface but more abrupt than in the solid interface, which suggests that the thermal stability of the atom motion or chain conformation transition in the model has been enhanced by the solid interface, but weakened by the free interface[31,48,49]. A glass transition behavior is observed in all three local regions. The T_gs of the solid interface, bulk and free interface are $T_{g,\,SV,\,solid}$ = 485 ± 13 K, $T_{g,\,SV,\,bulk}$ = 440 ± 17 K and $T_{g,\,SV,\,free}$ = 392 ± 15 K, respectively. The graphene surface triggers the bulk glass transition with a ~45 K higher T_g, while the vacuum restrains the bulk glass transition with a ~48 K lower T_g. Such asynchronous glass transition behaviors between interfacial and bulk regions can be attributed to the local volumetric heterogeneity of the film[50]. Comparing $T_{g,\,SV,\,solid}$, $T_{g,\,SV,\,bulk}$ and $T_{g,\,SV,\,free}$ (local T_g) with $T_{g,\,V}$ and $T_{g,\,FFV}$ (overall T_g) (Table 2), we find that $T_{g,\,V}$ and $T_{g,\,FFV}$ are both smaller than $T_{g,\,SV,\,bulk}$ and $T_{g,\,SV,\,solid}$ but larger than $T_{g,\,SV,\,free}$. The free interface offsets the effect of the solid interface on T_g increase and further reduced the overall T_g, suggesting that the free interface plays a stronger role in determining the overall T_g of the nanofilm[50]. The effect of the free interface on overall T_g can be reduced by decreasing the atomic mobility of both the free interface (e.g., increase bulk crosslink density) and the solid interface (e.g., graphene surface modification).

3.2.2. Energy Properties

To examine the energy contribution on the glass transition behavior of the model, the variations of both bonded and non-bonded energy components were monitored during cooling (Fig. 5). The bonded energies vary linearly with the decrease of the simulated temperature, suggesting that they do not contribute to the glass transition. This is consistent with previous reports for both linear and cross-linked polymers[46,51]. The non-bonded energy versus temperature exhibits a kink at $T_{g,\ nonbond}$ = 416 ± 9 K. After decomposition into electrostatic and van der Waals energies, the kink is observed only in the van der Waals energy at $T_{g,\ vdW}$ = 408 ± 7 K. The temperature dependency of the van der Waals energy is much more similar to that the total non-bonded energy, even though the electrostatic energy contributes a larger amount to the total non-bonded energy. Thus, the van der Waal energy serves as a major driving force for the glass transition of the system.

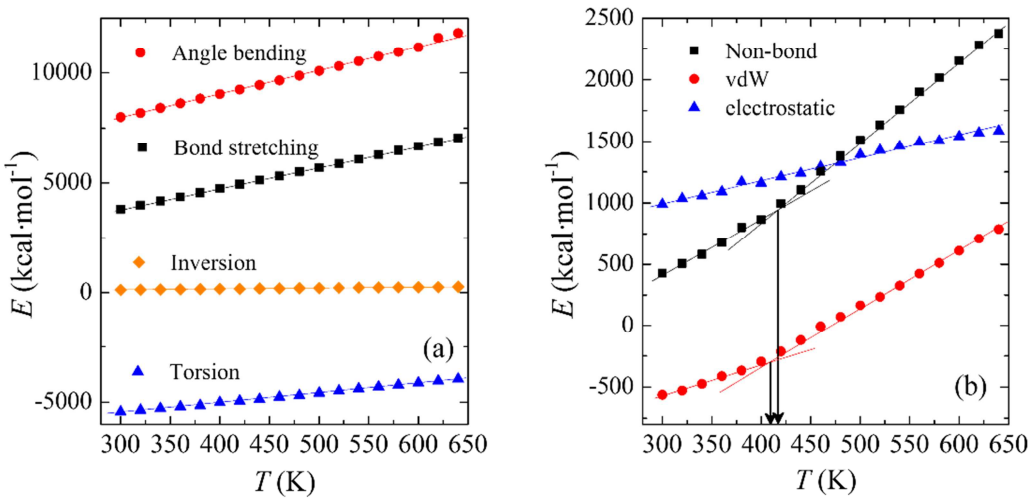

Fig. 5. Bonded (a) and non-bonded (b) potential energy components as a function of temperature.

The effect of the local non-bonded energy on the glass transition behavior was studied by

analyzing the variation of local hydrogen bond interactions along the *z* axis during cooling. Hydrogen bond energies cannot be obtained directly from the COMPASS force field. We use the average number of hydrogen bond (N_{HB}) instead. We use a geometric criterion for a hydrogen bond. The distance between hydrogen and acceptor is less than 2.5 Å and the donor-hydrogen-acceptor angle is less than 120º. N_{HB} is counted in the 10 Å thick slabs defined earlier and plotted as function of temperature (Fig. 6). N_{HB} in all slabs gradually increase during cooling. This may be attributed to decreasing free volume at lower temperature, which increases the odds for the formation of hydrogen bonds and less thermal fluctuations increasing the stability of the bonds[43,52]. The N_{HB} in all bulk slabs coincide with each other. N_{HB} in the 15~25 Å slab (solid interface) and the last 10 Å slab (free interface) are greater and less than bulk, respectively, indicating the heterogeneity also influences hydrogen bonding. The larger N_{HB} in the solid interface produces stronger internal binding force making this region more rigid than the bulk, while the fewer hydrogen bonds in the free interface allow more flexibility[52]. These observations are fully consistent with the results from the *SV-T* relations (Fig. 4).

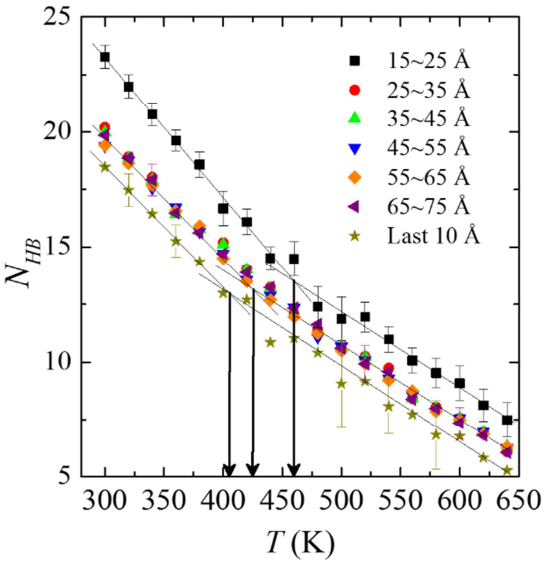

Fig. 6. Number of hydrogen bond in 7 representative 10 Å thick slabs in the film as a function of temperature. For clarity of details, not all error bars are shown.

All N_{HB} - T relations show a kink during the cooling, suggesting that the hydrogen bond energy also contributes to the glass transition behavior of the system and that hydrogen bonds can be used as a glass transition marker[53]. The T_g (HB) obtained from the linear fits of the glassy and rubbery regions are $T_{g,\,NB,\,solid}$ = 457 ± 11 K, $T_{g,\,NB,\,bulk}$ = 425 ± 13 K and $T_{g,\,NB,\,free}$ = 405 ± 19 K, respectively. Again the local non-bonded energy transitions in bulk and interfacial regions during the cooling process are asynchronous, in addition to the similar heterogeneous nature of the volume transitions discussed above. The hydrogen bonding based $T_{g,\,NB}$ values significantly deviate from the non-bonded energy based definition $T_{g,\,vdW}$ (408 K) or $T_{g,\,nonbond}$ (416 K), indicating that vdW interactions play a more important role than hydrogen bond interactions on the glass transition.

3.2.3. Dynamic Properties

To elucidate the relation between the glass transition and the dynamic properties, the *z* axis (normal) component of the mean square displacement, MSD_z, for all atoms was computed at each temperature. Then, the diffusion coefficient of the nanofilm along the film normal, D_z, was obtained from the slope of MSD_z - *t* plot in the time range of 200 ~ 800 ps. D_z and MSD_z were computed according to the following equation:[54]

$$D_z = \frac{1}{2}\lim_{t\to\infty}\frac{d(MSD_z)}{dt} = \frac{1}{2}\lim_{t\to\infty}\frac{d}{dt}\left\langle\left|\vec{r}_{z,i}(t)-\vec{r}_{z,i}(0)\right|^2\right\rangle \quad (1)$$

where $\vec{r}_{z,i}(t)$ denotes the position vector of *i*th particle and the angular brackets denote an ensemble average. The obtained MSD_z and D_z versus the simulated temperature are shown in Fig. 7. It should be noted that at large time, the MSD_z curves must reach an asymptotic value and the obtained D_zs should be zero for all temperatures, since monomers are confined in the z direction[55]. Therefore, the obtained results illustrate the intrinsic spatial and temporal fluctuations of dynamics that occurs in the nanofilm normal.

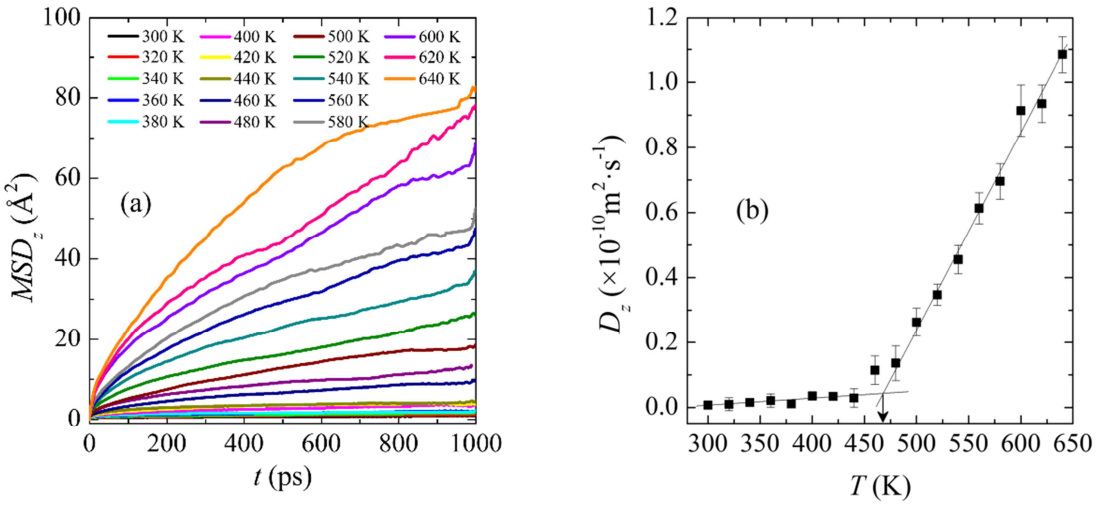

Fig. 7. Mobility of the polymer film as a function of temperature. (a) *z*-axis component of the mean square displacement (MSD_z) for all atoms in the system; (b) Diffusion coefficient of the

total nanofilm along *z* axis (D_z) of all atoms in the system.

The short time diffusive-like property obtained from the D_z - T relation indicates again a transition between two distinct stages for the dynamics in the nanofilm during cooling. In the higher temperature (rubbery) stage, the initial D_z value is relatively large but substantially drops with decreasing temperature. D_z is very small in the glassy state and almost temperature independent. There is a clear change of slope[35]. The almost vanishing diffusion in the glassy state shows that there is negligible mixing between layers as soon as the glass transition has occurred. By separately fitting the D_z data in the two stages, the $T_{g,\,D}$ is predicted to be 467 ± 13 K, which is significantly higher than the above obtained T_gs from volume and energy properties (Table 2). This is in good agreement with the results by Morita et al using a similar method[8,54]. They speculate that the glass transition suggested by dynamic properties is mainly due to the kinetic theory for structural relaxation, which is different with the mechanism of volume or energy. It is noteworthy that due to the higher temperature for dynamical arrest, layers will not mix anymore even if we are above the structural glass transition.

The kink of the D_z - T relation near T_g suggests that the glass transition behavior depends largely on the thermal motion of atoms along the *z* axis of the film. More detailed information about the heterogeneous dynamic property of the nanofilm along *z* axis is needed to obtain a further understanding of the local glass transition mechanism. To this end, the *z* axis component of the mean square fluctuation tensor ($R_{g,\,z}$) over a period of 500 ps along the trajectory was computed. The central carbon atoms on the epoxy monomers are taken as representation of the monomers. A larger $R_{g,\,z}$ indicates that the atom in the model has a

greater range of motion, i.e., larger mobility. $R_{g,z}$ can be calculated as:[30]

$$R_{g,z} = \sqrt{\frac{1}{N}\sum_{i}^{N} | \vec{r}_{z,i} - \vec{r}_{z,mean} |^2} \quad (2)$$

where N is the number of snapshots in the trajectory, $\vec{r}_z$ and $\vec{r}_{z,mean}$ are the position vector in ith snapshot and the mean position vector along the trajectory, respectively. The nanofilm was again divided into several 10 Å thick slabs along the z axis and the $R_{g,z}$ of the representative carbon atoms in each slab was calculated as a function of temperature (Fig. 8).

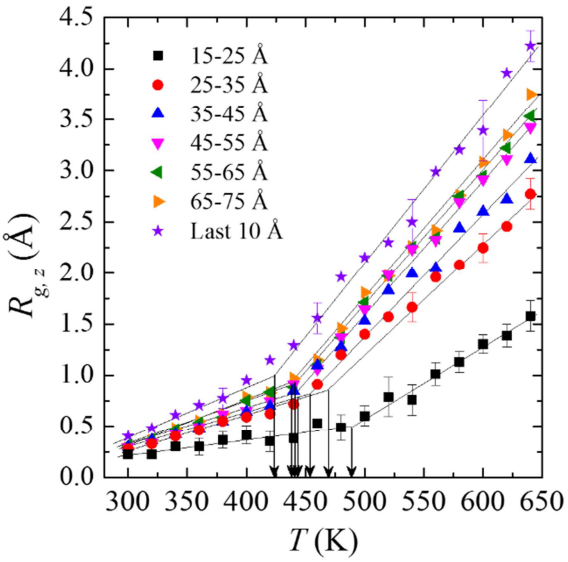

Fig. 8. Normal component of the mean square fluctuation tensor for central carbon atoms on epoxy monomers in 7 representative 10 Å thick slabs of the nanofilm as a function of temperature. For clarity of details, not all error bars are shown.

In general, as the temperature decreases, the $R_{g,z}$ for each local slab of the nanofilm is reduced and again this reduction process is separated into two stages, indicating a glass transition at each region[56]. As expected, at each temperature, the $R_{g,z}$ of the 15 ~ 25 Å slab is the smallest, while the $R_{g,z}$ of the last 10 Å slab is the largest in agreement with *SV* (Fig. 4)

and N_{HB} (Fig. 6), which indicates that the graphene surface and vacuum separately restrain and enhance the mobility of atoms in the solid and free interfaces, respectively. However, unlike SV and N_{HB}, the $R_{g,z}$ values for the 5 slabs from 25 Å to 75 Å do not coincide very well. The local glass transition of all considered slabs are influenced by the solid surface to a different extent[50,56]. As the 3 slabs between 45 and 75 Å behave very similar, we can define a much broader solid interface region. We almost see a continuous increase of mobility away from the surface. Thus, the thickness of the solid interface is less well defined and closer to 30 Å, which is larger than the extent of the mass density peak range (15 Å) in Fig. 2. We mainly attribute this large disparity to the complex chain configurations of the epoxy monomers in the nanofilm. The relative larger extension of the solid interface region also explains why T_g values predicted by dynamic ($T_{g,D}$ = 467 ± 13 K, $T_{g,P}$ = 460 ± 20 K) are much larger than that by volume ($T_{g,V}$ = 422 ± 11 K, $T_{g,FFV}$ = 412 ± 7 K) and energy ($T_{g,nonbond}$ = 416 ± 9 K, $T_{g,vdW}$ = 408 ± 7 K). Moreover, the $R_{g,z}$ values at higher temperatures have shown much larger deviation than at lower temperatures, especially for the two slabs from 25 Å to 45 Å. This indicates that the influence range of the solid graphene surface is extended at higher temperatures.

There is an obvious gap between the 15 Å to 25 Å slab and the 25 Å to 35 Å slab at all temperatures. The thermal motion of atoms in the 15 Å to 25 Å slab suffer from stronger restriction than other local regions of the solid interface due to the attraction force and steric hindrance of the solid surface. Beyond this slab, the dynamic width of the solid interface has been largely extended by penetrating into the bulk region[56]. Therefore, it is speculated that there is a dynamical “locked” slab within the solid interface region among the simulated

temperature range. Fig. 9 shows a schematic illustration for the interfacial and bulk regions in the nanofilm. Here, the solid interface region is separated into a "locked" slab and a penetration region. This slab shows similar glass transition phenomenon with other slabs. The $T_{g,\,Rg}$ values for slabs from the graphene surface to the vacuum are predicted to be 488 ± 13, 469 ± 18, 454 ± 16, 443 ± 13, 440 ± 11, 437 ± 11, 423 ± 23 K, respectively. Here, the "locked" slab mainly attributes to the large $T_{g,\,D}$ value (467 ± 13 K, Fig. 7) of the overall nanofilm, while the slabs from 35 Å to the vacuum contribute to the decrease of $T_{g,\,D}$. Thus, this specific local region plays a specific role in restraining the thermodynamic properties of atoms during glass transition[21]. Overall, the local dynamic properties of the nanofilm are much more variable and complicated than the volume and energy properties. The variations of $R_{g,\,z}$ and T_g value distributions in different local regions along *z* axis prove that there is large dynamic heterogeneity along the film normal[57]. The heterogeneity is considered as the driving force for the dynamical percolation of the total nanofilm along the *z* axis, and the "locked" slab is treated as the initiator and accelerator of the dynamical percolation.

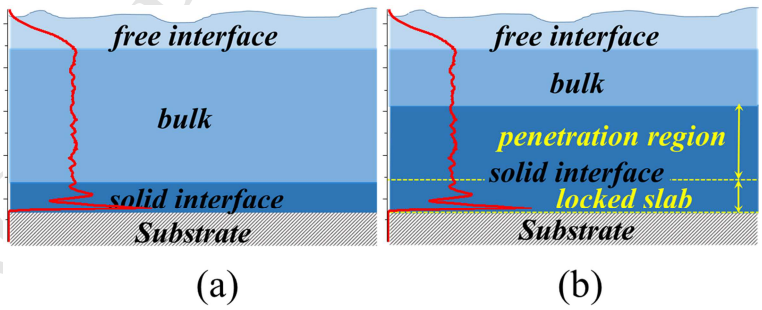

Fig. 9. Schematic illustration for the position of the solid interface, bulk and free interface regions obtained from the (a) volume, energy properties and (b) dynamic properties. The red lines represent the general distribution of mass density in the nanofilm.

3.3. Percolation of the Nanofilm during Glass Transition

The dynamic percolation of the nanofilm along the *z* axis has been explored to further demonstrate the effect of heterogeneous properties on the overall glass transition behavior. A previously suggested approach was used to classify the system into mobile or immobile domains[22,30]. First, the radial distribution function (RDF) of the central carbons representing the epoxy monomers was computed at different temperatures and the first peak and minimum positions are temperature dependent at 6.30 Å and 9.75 Å, respectively (Fig. 10a). An atom was defined to be immobile if its $R_{g,\,z}$ is smaller than one-tenth of the distance to the first RDF peak (0.63 Å). Each immobile atom was considered to occupy a sphere of diameter 9.75 Å. If two spheres overlap, they are treated as part of the same immobile domain. If any domain was large enough to extend from the solid interface to the free interface, the system is considered to be percolated by immobile domains. Fig. 10b shows the computed percolation probability (*P*) of the representative central carbon atoms on epoxy monomers as a function of temperature. The total evolution of *P* is separated into three stages during cooling. At temperatures larger than 460 K or smaller than 360 K, *P* is 0 or 1, indicating a non-percolated state and total percolation, respectively. The transition of *P* from 0 to 1 describes the evolution of the model from non-percolated to total percolation. The large uncertainty of *P* during the percolation process can be attributed to large dynamical heterogeneity of the model near T_g[29,30], while the small uncertainty of *P* at temperatures lower than 340 K indicates a highly percolated nature of the model at glassy state.

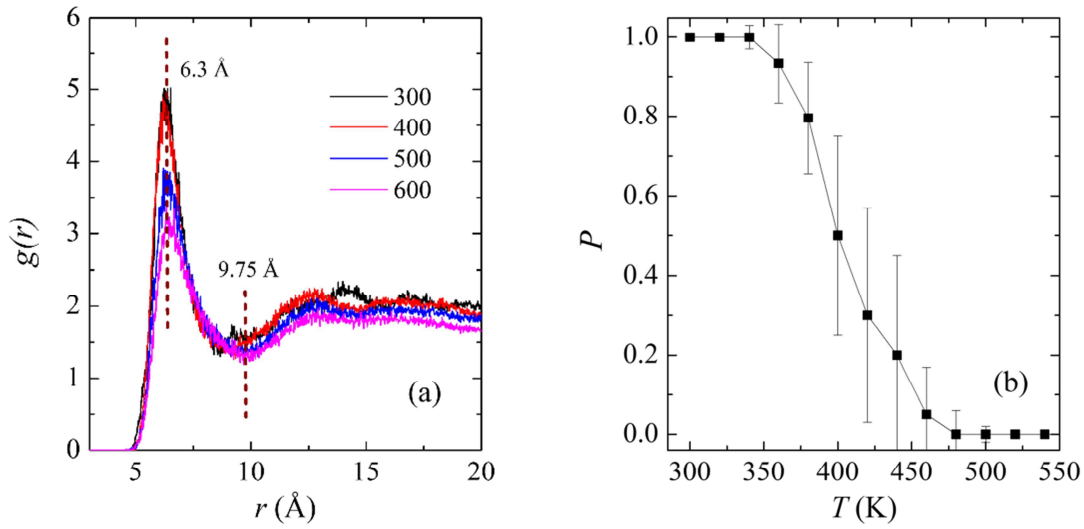

Fig. 10. Dynamical percolation of the system. (a) Distances criteria from RDF of the central carbon atoms in the system; (b) Percolation probability of the system as a function of temperature.

To visually demonstrate the internal percolation status of the nanofilm system during cooling, the $R_{g,z}$ size distributions of the representative carbon atoms were depicted by a specific color scheme (Fig. 11). Colors from deep blue to deep red (i.e., $R_{g,z}$ values from 0 Å to >5 Å) represent the variation of atom clusters from immobile to mobile. Generally, the diagram is separated into various colored domains at each simulated temperature, which represents the internal dynamic heterogeneous nature of the nanofilm. In particular, a non-uniform distribution trend is found along the z axis as the solid surface and vacuum will make domains more immobile and mobile, respectively. A particular blue domain is observed near the solid surface at all temperatures, supporting the existence of the "locked" slab in the solid interface region (Fig. 9). The nanofilm exhibits a larger $R_{g,z}$ range (i.e., color range) at higher temperatures than at lower temperatures due to the existence of both a "locked" slab and

highly mobile surface domains. For example, the diagram at 640 K shows a $R_{g,z}$ range from 0 to 5 Å, while at 300 K a much smaller $R_{g,z}$ range from 0 to 0.5 Å. Such temperature dependent heterogeneous variation is closely related to the chemical or physical characteristics of the polymeric materials and the interfacial bonding strength between the solid surface and the nanofilm[58,59]. Therefore, the molecular or structural design of nanofilm materials with precisely controlled microscopic dynamic heterogeneity is of great significance according to their performance requirements in industrial applications.

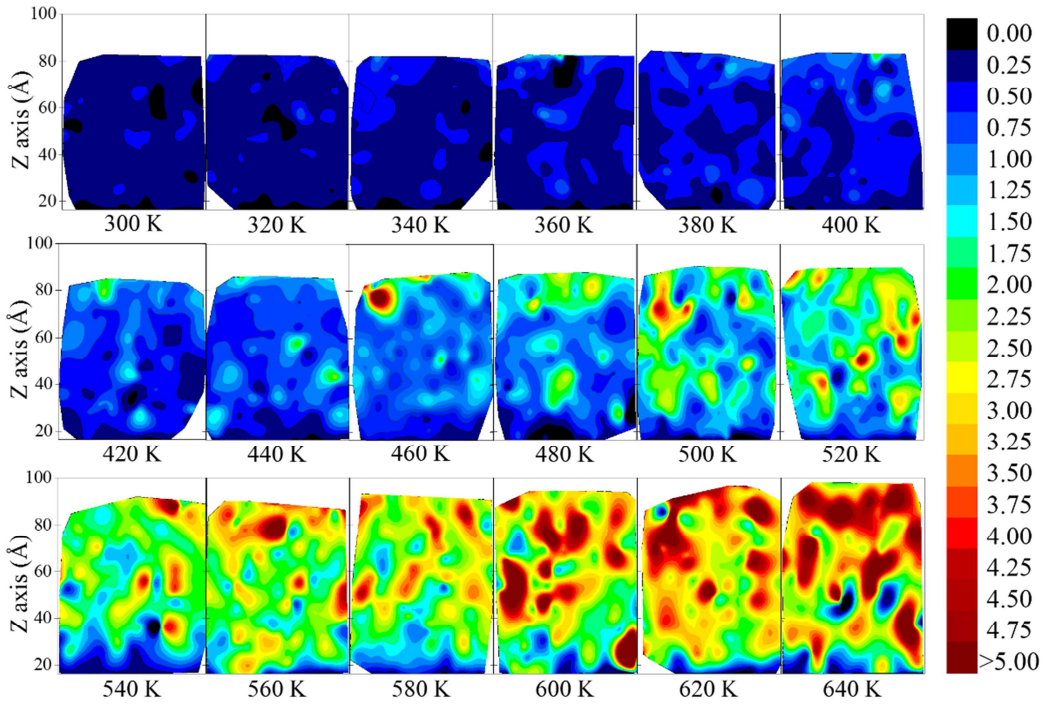

Fig. 11. R_g domain distributions for the central carbon atoms on epoxy monomers in the system during cooling. The horizontal and vertical axes of these Fig.s represent X and Z axes of the model, respectively. Graphene layers are not shown.

During cooling, the transformation of the colored diagram follows two basic rules: (1) larger interconnected red (mobile) domains are gradually separated into smaller domains before

they finally disappear; (2) smaller dispersed blue (immobile) domains collide with each other and gradually merge into larger domains. To better understand the percolation of the nanofilm during the glass transition process, the entire cooling process is separated into six different stages. Stage 1 (highly rubbery): the nanofilm only has a small fraction of relatively immobile domains near the solid surface and has a large thermal mobility range along *z*. Stage 2 (low rubbery): the nanofilm has relatively immobile domains near the solid surface and a certain fraction of relatively immobile domains scattered in the bulk region. Stage 3 (onset of glass transition): the scattered immobile domains interconnect and form a bridge between the solid interface region and the free interface region, percolation starts. Stage 4 (glass transition strengthens): more bridges appear and form network-like internal paths between the solid interface region to the free interface region and a high percolation probability is reached. Stage 5 (low glassy): immobile domains have a high interconnection degree and there is still a small fraction of mobile domains. Stage 6 (high glassy state): the entire nanofilm is one united immobile domain and the thermal mobility range along *z* axis becomes extremely small. These stages are schematically displayed in Fig. 12.

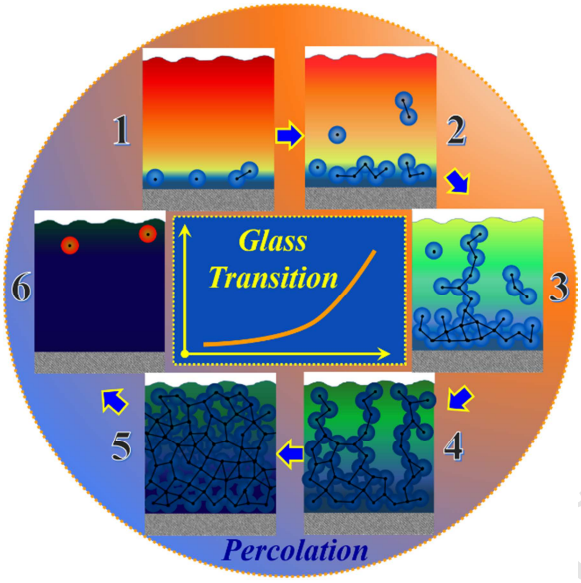

Fig. 12. Schematic illustration for the percolation process of the nanofilm by immobile domains during the cooling process. Blue circles indicate immobile domains, and the black lines between blue circles denotes the interconnection of these domains. Red circles in stage 6 indicate a small fraction of relative mobile domains. Background colors from bright (deep red) to dark (deep blue) indicate domains with high and low atomic mobility, respectively.

Before the percolation onset, the "locked" domain in the nanofilm serves as precursor and stimulus for the percolation of the bulk and free interface regions during cooling. Most immobile domains start near the "locked" domain and then penetrate upward as the temperature decreases[59]. Also, as the "locked" domain depends on the solid surface, we speculate that the modification of solid surface (e.g., interface grafting) has a big influence on the volume of the "locked" domain and then affects the overall percolation of the nanofilm[17,21,22,28]. Then, the system will start percolating (i.e., P starts to increase at $T_{g,P}$ = 460 K) when an immobile domain with a specific $R_{g,z}$ value is large enough to partially connect the solid interface region and free interface region[30]. From the 460 K diagram in Fig.

11, it is roughly estimated that the system is partially percolated by blue domains with $R_{g,z}$ ranges from 0.5 Å to 1.0 Å. From the $R_{g,z}$ - T relations in Fig. 8, the T_g values are basically obtained within a similar range of $R_{g,z}$. Therefore, the T_g of the nanofilm is closely related to the temperature when the system starts to percolate. This is in good agreement with previously reported simulation studies on both pure epoxy or epoxy based nanocomposite materials[22,30]. Finally, after percolation, the highly interconnected bridges in the nanofilm will make a joint effect on the local or overall properties of the system[59]. This will make it harder to further decrease the volume, energy and dynamic properties of the system.

4. Conclusions

In the present work, the heterogeneous and percolation properties of an epoxy nanofilm, located on a 4-layer-graphene surface, were studied during glass transition by all-atom molecular dynamics simulations. To this end, the temperature dependent volume, energy and dynamic properties in both overall and local aspects were analyzed in detail at different temperatures. A layered solid interface region, a constant bulk region and a density dropping free interface region are found successively along the film normal. Local properties of specific volume (SV), hydrogen bond number (N_{HB}) and motional gyration radius (R_g) further indicate the heterogeneous nature of the nanofilm, in which studies on R_g give a much thicker solid interface region (~ 30 Å) than that on SV and N_{HB} (~ 10 Å). The heterogeneous feature is reflected by the asynchronous glass transition behaviors of local regions during the cooling process. Local structure, energy and dynamic studies highlight the significance of three individual regional glass transitions at the solid interface (high T_g), bulk (moderate T_g) and free interface (low T_g) regions for the overall thermodynamic property of the nanofilm. With

cooling of the model, the internal glass transition develops from a relatively immobile (locked) region near the graphene surface to the bulk and finally the free interface, during which small dispersed immobile domains collide with each other and gradually merge into large interconnected domains, i.e., percolation along z axis. This evolution is triggered by the locked region near the solid surface and accelerated by newly percolated domains at temperatures near T_g. We developed a detailed evolution mechanism consisting of six different stages according to the internal percolation status of the system. This mechanism provides a theoretical guide to interpret the glass transition behavior and will be useful to guide the design and fabrication of nanofilm materials in experiments.

ACKNOWLEDGMENTS

The authors gratefully acknowledge the financial support of the Fundamental Research Funds for the Central Universities (14CX02221A, 16CX06023A and 16CX05017A), and the Applied Fundamental Research Foundation of Qingdao Independent Innovation Plan (15-9-1-46-jch and 16-5-1-90-jch).

REFERENCES

[1] Jin, K.; Torkelson, J. M. *Macromolecules* **2016**, 49, 5092-5103.

[2] Boucher, V. M.; Cangialosi, D.; Yin, H.; Schönhals, A.; Alegría, A.; Colmenero, J. *Soft Matter* **2012**, 8, 5119-5122.

[3] Forrest, J.; Dalnoki-Veress, K.; Dutcher, J. *Physical Review E* **1997**, 56, 5705.

[4] Forrest, J.; Dalnoki-Veress, K.; Stevens, J.; Dutcher, J. *Physical Review Letters* **1996**, 77, 2002.

[5] Pye, J. E.; Roth, C. B. *Journal of Polymer Science Part B: Polymer Physics* **2015**, 53, 64-75.

[6] Hu, W.; Patil, N. V.; Hsieh, A. J. *Polymer* **2016**, 100, 149-157.

[7] Patrone, P. N.; Dienstfrey, A.; Browning, A. R.; Tucker, S.; Christensen, S. *Polymer* **2016**, 87, 246-259.

[8] Morita, H.; Tanaka, K.; Kajiyama, T.; Nishi, T.; Doi, M. *Macromolecules* **2006**, 39, 6233-6237.

[9] Pu, J.; Mo, Y.; Wan, S.; Wang, L. *Chemical Communications* **2014**, 50, 469-471.

[10] Berman, D.; Erdemir, A.; Zinovev, A. V.; Sumant, A. V. *Diamond and Related Materials* **2015**, 54, 91-96.

[11] Chen, L.; Torkelson, J. M. *Polymer* **2016**, 87, 226-235.

[12] Casalini, R.; Zhu, L.; Baer, E.; Roland, C. *Polymer* **2016**, 88, 133-136.

[13] Ediger, M.; Forrest, J. *Macromolecules* **2013**, 47, 471-478.

[14] Biroli, G.; Garrahan, J. P. *The Journal of Chemical Physics* **2013**, 138, 12A301.

[15] Schönhals, A.; Zorn, R.; Frick, B. *Polymer* **2016**, 105, 393-406.

[16] Oh, H.; Green, P. F. *Nature Materials* **2009**, 8, 139-143.

[17] Pastorino, C.; Binder, K.; Kreer, T.; Müller, M. *The Journal of Chemical Physics* **2006**, 124, 064902.

[18] Yang, Z.; Fujii, Y.; Lee, F. K.; Lam, C.-H.; Tsui, O. K. C. *Science* **2010**, 328, 1676-1679.

[19] Chai, Y.; Salez, T.; McGraw, J. D.; Benzaquen, M.; Dalnoki-Veress, K.; Raphaël, E.; Forrest, J. A. *Science* **2014**, 343, 994-999.

[20] Fakhraai, Z.; Forrest, J. A. *Science* **2008**, 319, 600-604.

[21] Wang, Z.; Lv, Q.; Chen, S.; Li, C.; Sun, S.; Hu, S. *ACS Applied Materials & Interfaces* **2016**, 8, 7499-7508.

[22] Khare, K. S.; Khabaz, F.; Khare, R. *ACS Applied Materials & Interfaces* **2014**, 6, 6098-6110.

[23] Eslami, H.; Müller-Plathe, F. *The Journal of Physical Chemistry C* **2013**, 117, 5249-5257.

[24] Ghanbari, A.; Ndoro, T. V. M.; Leroy, F.; Rahimi, M.; Böhm, M. C.; Müller-Plathe, F. *Macromolecules* **2012**, 45, 572-584.

[25] Li, C.; Strachan, A. *Journal of Polymer Science Part B: Polymer Physics* **2015**, 53, 103-122.

[26] Guseva, D. V.; Komarov, P. V.; Lyulin, A. V. *Journal of Polymer Science Part B: Polymer Physics* **2016**, 54, 473-485.

[27] Wu, C. *Journal of Polymer Science Part B: Polymer Physics* **2017**, 55, 178-188.

[28] Ndoro, T. V. M.; Böhm, M. C.; Müller-Plathe, F. *Macromolecules* **2012**, 45, 171-179.

[29] Long, D.; Lequeux, F. *The European Physical Journal E* **2001**, 4, 371-387.

[30] Lin, P.-H.; Khare, R. *Macromolecules* **2010**, 43, 6505-6510.

[31] Khare, K. S.; Khare, R. *The Journal of Physical Chemistry B* **2013**, 117, 7444-7454.

[32] Castillo, F. Y.; Socher, R.; Krause, B.; Headrick, R.; Grady, B. P.; Prada-Silvy, R.; Pötschke, P. *Polymer* **2011**, 52, 3835-3845.

[33] Lipson, J.; Milner, S. *The European Physical Journal B* **2009**, 72, 133-137.

[34] Kropka, J. M.; Pryamitsyn, V.; Ganesan, V. *Physical Review Letters* **2008**, 101, 075702.

[35] Wang, Z.; Lv, Q.; Chen, S.; Li, C.; Sun, S.; Hu, S. *Molecular Simulation* **2015**, 41,

1515-1527.

[36] Shuichi, N. *Progress of Theoretical Physics Supplement* **1991**, 103, 1-46.

[37] Swope, W. C.; Andersen, H. C.; Berens, P. H.; Wilson, K. R. *The Journal of Chemical Physics* **1982**, 76, 637-649.

[38] Sun, H. *The Journal of Physical Chemistry B* **1998**, 102, 7338-7364.

[39] Ewald, P. *Ann. Phys* **1921**, 64, 253-287.

[40] Hanakata, P. Z.; Douglas, J. F.; Starr, F. W. *The Journal of Chemical Physics* **2012**, 137, 244901.

[41] Voyiatzis, E.; Rahimi, M.; Müller-Plathe, F.; Böhm, M. C. *Macromolecules* **2014**, 47, 7878-7889.

[42] Liu, H.; Li, M.; Lu, Z.-Y.; Zhang, Z.-G.; Sun, C.-C.; Cui, T. *Macromolecules* **2011**, 44, 8650-8660.

[43] White, R. P.; Lipson, J. E. G. *Macromolecules* **2016**, 49, 3987-4007.

[44] Fox, T.; Loshaek, S. *Journal of Polymer Science* **1955**, 15, 371-390.

[45] Sharma, S. K.; Sudarshan, K.; Sahu, M.; Pujari, P. K. *RSC Advances* **2016**, 6, 67997-68004.

[46] Yang, S.; Qu, J. *Polymer* **2012**, 53, 4806-4817.

[47] Putz, K. W.; Palmeri, M. J.; Cohn, R. B.; Andrews, R.; Brinson, L. C. *Macromolecules* **2008**, 41, 6752-6756.

[48] Polizos, G.; Tuncer, E.; Agapov, A. L.; Stevens, D.; Sokolov, A. P.; Kidder, M. K.; Jacobs, J. D.; Koerner, H.; Vaia, R. A.; More, K. L.; Sauers, I. *Polymer* **2012**, 53, 595-603.

[49] Lin, P.-H.; Khare, R. *J Therm Anal Calorim* **2010**, 102, 461-467.

[50] White, R. P.; Price, C. C.; Lipson, J. E. G. *Macromolecules* **2015**, 48, 4132-4141.

[51] Wu, C.; Xu, W. *Polymer* **2007**, 48, 5802-5812.

[52] Qin, X.; Xia, W.; Sinko, R.; Keten, S. *Nano Letters* **2015**, 15, 6738-6744.

[53] Kim, G.-H.; Lee, D.; Shanker, A.; Shao, L.; Kwon, M. S.; Gidley, D.; Kim, J.; Pipe, K. P. *Nat Mater* **2015**, 14, 295-300.

[54] Meunier, M. *The Journal of Chemical Physics* **2005**, 123, 134906.

[55] Ghosh, J.; Faller, R. *The Journal of Chemical Physics* **2006**, 125, 044506.

[56] Ndoro, T. V.; Böhm, M. C.; Müller-Plathe, F. *Macromolecules* **2011**, 45, 171-179.

[57] Siretanu, I.; Saadaoui, H.; Chapel, J.-P.; Drummond, C. *Macromolecules* **2015**, 48, 2787-2792.

[58] Rijal, B.; Delbreilh, L.; Saiter, A. *Macromolecules* **2015**, 48, 8219-8231.

[59] Körner, M.; Prucker, O.; Rühe, J. *Macromolecules* **2016**, 49, 2438-2447.

Highlights:

- Film heterogeneity manifests in overall and local volume, energy and dynamic
- Solid and free interfaces foster asynchronous glass transition of the nanofilm
- Percolation of immobile domains relates glass transition to film heterogeneity
- Immobile domains initiate and accelerate film percolation during glass transition